Water Research 185 (2020) 116287

Contents lists available at ScienceDirect

Water Research

journal homepage: www.elsevier.com/locate/watres

Nonintrusive investigation of large Al-kaolin fractal aggregates with slow settling velocities

Rodrigo B. Moruzzi[a,b,d,*], Luiza C. Campos[b], Soroosh Sharifi[c], Pedro Grava da Silva[d], John Gregory[b]

[a] Instituto de Geociências e Ciências Exatas, Univ. Estadual Paulista (UNESP), Av. 24-A, 1515, Jardim Bela Vista, Rio Claro, 13506-900. São Paulo, Brazil
[b] Department of Civil, Environmental and Geomatic Engineering, University College London, Gower St, London WC1E 6BT, United Kingdom
[c] Department of Civil Engineering, University of Birmingham, B15 2TT, United Kingdom
[d] Programa de Pós-graduação em Engenharia Civil e Ambiental, Univ. Estadual Paulista (UNESP), Av. 24-A, 1515, Jardim Bela Vista, Rio Claro, São Paulo 13506-900. Brazil

Nonintrusive Investigation of Large Al-kaolin Fractal Aggregates with Slow Settling Velocities

Rodrigo B. Moruzzi[a*], Luiza C. Campos[b], Soroosh Sharifi[c], Pedro Grava da Silva[d], John Gregory[b]

[a] Instituto de Geociências e Ciências Exatas, Univ. Estadual Paulista (UNESP), Av. 24-A, 1515, Jardim Bela Vista, Rio Claro, 13506-900. São Paulo, Brazil. E-mail: rodrigo.moruzzi@unesp.br

[b] Department of Civil, Environmental and Geomatic Engineering, University College London, Gower St, London, WC1E 6BT, United Kingdom. E-mail: l.campos@ucl.ac.uk ; j.gregory@ucl.ac.uk

[c] Department of Civil Engineering, University of Birmingham, B15 2TT, United Kingdom. Email: S.Sharifi@bham.ac.uk

[d] Programa de Pós-graduação em Engenharia Civil e Ambiental, Univ. Estadual Paulista (UNESP), Av. 24-A, 1515, Jardim Bela Vista, Rio Claro, 13506-900. São Paulo, Brazil. E-mail: pedroagrava@gmail.com

Address:

* Corresponding author: Avenida 24-A, nº 1515, C. P. 178, CEP 13506-900, Office 23, Bela Vista, Rio Claro, São Paulo, Brazil. Phone: +55 19 3526-9339. *E-mail address*: rodrigo.moruzzi@.unesp.br

Abstract

Although a combination of aggregate characteristics dictate particle settling, it is commonly assumed that large particles have higher terminal velocities. This simplifying assumption often leads to overprediction of large aggregate settling velocities which in turn negatively impacts on estimates of sedimentation clarification efficiency. Despite its importance, little attention has been given to large aggregates with slow-settling velocities. This paper addresses this gap by investigating slow-settling velocities of large, heterodisperse and multi-shape Al-kaolin aggregates using non-intrusive methods. A particle image velocimetry technique (PIV) was applied to track aggregate velocity and a non-intrusive image technique was used to determine aggregate characteristics, including size (d_f), three-dimensional fractal dimension (D_f), density (ρ_f), aggregate velocity (V_{exp}) and Reynolds number (Re). Results showed no strict dependence of settling velocity on large aggregate size, shape and density, as Al-kaolin aggregates with the same size exhibited different settling velocities. A comparison of the results with the well-known Stokes' law for velocity modified by a shape factor showed that the settling velocities measured here can vary from 2 to 14 fold lower than the predicted values for perfect sphere-shape aggregates with the same density and size. Furthermore, results have also shown large Al-kaolin aggregate's drag coefficient (Cd) to be around $56/Re$, for average fractal aggregate sphericity of around 0.58.

Keywords: flocculation, fractal dimension, settling velocity, aggregate density, sedimentation

1- Introduction

Sedimentation is widely used as a technique for separating suspended material in water treatment before filtration. This stage is commonly preceded by coagulation and flocculation processes, which destabilize colloids and promote their subsequent agglomeration, favouring the formation of large aggregates, which are commonly assumed as more likely to settle in sedimentation tanks. This comes from the belief that size and density are dependent features and that aggregates can be considered as spheres, as described by Stokes' law. However, some studies (e.g. Chakraborti et al., 2000; Johnson, Li and Logan, 1996; Vahedi and Gorczyca, 2014) have shown that the complex mechanisms involving aggregation, breakage, restructuring of multi-shape primary particles and different relations between size, shape and density can result in different terminal settling velocities, even for fractal aggregates with the same size. As such, practitioners have reported that large aggregates may still remain in the supernatant water due to their very slow-settling velocity, which can be attributed to features other than their size (Vahedi and Gorczyca, 2012).

The aggregates formed from the flocculation of colloidal material are known as fractal objects (Jiang and Logan, 1991; Gregory, 1997), i.e. they have non-spherical shape and porous structures, and hence, cannot be fully geometrically represented by a sphere. Despite this, to reduce the complexities of aggregate settling hydrodynamics, it is still common to evaluate the sedimentation of particles by assuming impervious and perfect-shape sphere aggregates (Bushell et al., 2002). It is known that this oversimplification may lead to inaccurate predictions of settling velocity with significant errors, with actual velocity estimates varying from 4 to 8 times higher, as shown by Johnson et al. (1996) to 5 times lower, as shown by Vahedi and Gorczyca (2012). This makes it difficult to fully understand the phenomena and their relevance to engineering (Johnson et al., 1996, Gregory, 1997, Li et al., 2006 and Vahedi and Gorczyca, 2012). Therefore, for practical reasons, it is necessary to gain a better understanding of the complex relation between the characteristics of large fractal aggregates produced by coagulation and flocculation, and their settling velocities.

Fractal dimension can be related to aggregates' porosity, density, strength of flocs, sedimentation velocity, collision models and flocculation kinetics. Settling velocity is mainly dependant on the density and size of aggregates, which in turn may be strongly affected by the interrelated parameters of porosity and permeability. Low fractal dimensions change the density-size relationship, thus affecting aggregate mass, whereas higher porosity may also affect flocs permeability, favouring water flow through flocs, and decreasing flow resistance. Some studies incorporated the understanding of fractal geometry into the dynamics of aggregate removal. Gregory (1997) and Jarvis et al., (2005) followed a theoretical and conceptual approach, while Vahedi and Gorczyca (2014) focused on modelling and simulation. So far, few papers have combined experimental with fundamental approaches (e.g. Johnson et al., 1996; Tang et al., 2002; Vahedi and Gorczyca, 2012, Chakraborti and Kaur, 2014).

In terms of floc size and settling velocity, Vahedi and Gorczyca (2012) have studied lime softening flocs (denser than Alum flocs), where an average of 2.37×10^{-3} $m\cdot s^{-1}$ was measured for an average size of 124 μm of equivalent diameter. However, this settling velocity was slower than those presented by Johnson et al. (1996), who have studied fractal aggregates (2 - 40 μm) formed from latex microspheres, and coagulated with NaCl solution at a shear rate of 5 s^{-1}. Johnson et al. (1996) found settling velocities to be 4 to 8 times higher than Stokes' law prediction, i.e. 1.0×10^{-4} to 1.0×10^{-3} $m\cdot s^{-1}$. These results differ from the expected ones, and it is difficult to explain why such high velocities were measured, even considering high permeability and the flow-through floc effect, as pointed by Bushell et al. (2002). Although primary particles in real flocs are heterodisperse and multi-shaped, latex spheres of known sizes were still used in many of these works to form aggregates. Nevertheless, Chakraborti and Kaur (2014) have also shown that even for large latex spheres (size larger than 100 μm) settling velocities may also be lower than those predicted by Stokes' law equation. They concluded that drag coefficients (Cd) assumed in the Stokes' law velocity expression may be not applicable for larger particles, even with $Re < 1$. Furthermore, primary particles affect aggregates' shape and there is evidence that large aggregates have fractal-like shapes, with lower dimensions, resulting in lower density compared to smaller aggregates (Johnson et al., 2016; Vahedi and Gorczyca, 2012 and Moruzzi et al., 2017). According to Bushell et al. (2002), the impact of aggregation of primary particles on hydrodynamics may result either in the increase of drag forces compared to spherical primary particles, or in the formation of aggregates that can become permeable, decreasing the drag force. This may impact the settling velocity and more investigation is needed to confirm which effect prevails on large aggregates.

This study aims to systematically investigate and analyse the features and dynamics of slow settling Al-kaolin fractal large aggregates. The focus here is specifically, large, heterodisperse and multi-shape flocculated kaolin particles settled by gravity. To avoid the assumption that particle size and drag force are intrinsically related, a non-intrusive imaging method has been used as a means to characterise aggregates' behaviour, rather than settling velocity. Particle image velocimetry (PIV) is used to measure aggregates' settling velocity as well as their size and shape. Furthermore, a novel procedure is applied to convert 2D fractal dimensions into

3D from image analysis. Size and density were analysed and correlated from two approaches, individually and from the entire population of aggregates. The shape, Reynolds number and drag coefficients of large Al-kaolin fractal aggregate velocities are determined, and experimental velocities are compared with estimates using Stokes' equation modified by a shape factor, which has been widely used in predicting settling velocities.

2- **Methodology**

2.1 Synthetic water preparation

For the present study, commercial kaolin (Sigma-Aldrich) was used as primary particle and synthetic water was prepared from a stock suspension (turbidity 5000 ± 200 NTU), as recommended by Yukselen and Gregory (2004). For each assay, a volume of 10 mL from stock solution was diluted in 2 L of deionized water to produce water with turbidity 25 ± 2 NTU (15.8 ± 1.3 mg TSS$\cdot$ L^{-1}), as previously investigated by Moruzzi et al. (2017). This range of low-to-medium turbidity was selected to represent conditions found in many freshwater sources during dry seasons, e.g. in Sao Paulo State, Brazil (CETESB, 2015) or in the USA (Swenson, 1965), respectively. This type of water has been also studied by other researchers (e.g. Li et al., 2008; Wei et al., 2010; Liu et al., 2019; Eman et al., 2010). A MALVERN Mastersizer 2000 particle size analyser and a Scanning Electron Microscope (SEM) were used to measure kaolin size distribution and to define the representative pixel size, i.e. the ratio between image resolution and size that better describes flocs, for the kaolin bulk particles which form the aggregates, as discussed by Moruzzi et al. (2017). Analytical grade alum ($Al_2(SO_4)_3\cdot 14\cdot H_20$) from Sigma-Aldrich was used as coagulant and analytical grade sodium bicarbonate (0.1 M, $NaHCO_3$) was used as a pH buffer during coagulation tests. Here, the coagulation conditions obtained by

Oliveira et al. (2015) and Moruzzi et al. (2017) were applied, i.e. 2 mg Al·L^{-1} and pH of 7.5. The aggregates were obtained after flocculation with velocity gradients (G_f) ranging from 20 to 60 s^{-1} for 15 minutes of flocculation time in order to consider aggregates of different sizes and shapes. The sedimentation vessel had a cross-sectional area of 150 × 150 mm. The temperature was kept at about 20 ± 1 ºC during all experiments.

2.2 Non-intrusive image analysis

To study large aggregates with slow settling velocity, only the ones that remained in the supernatant after 5 minutes of sedimentation were monitored. This meant that only aggregates with settling velocities slower than 4.6 ×10^{-4} m·s^{-1} (40 m·day^{-1}) would remain in the sampling point, which is equivalent to the loading rate of conventional settling tanks. Furthermore, low aggregates remain in the supernatant and therefore minor hydrodynamic interference can be assumed (Goula et al. 2008). This was also to ensure minimum inertial fluid motion after flocculation, and the predominance of aggregate vertical trajectory. In total, 118 aggregates were individually monitored applying a non-intrusive image acquisition system using a *High-Speed Miro EX-4* camera with interchangeable lenses. This approach avoids the assumption of an explicit relationship between drag coefficient and aggregate size, as mentioned by Bushell et al. (2002).The lighting system was set up as proposed by Moruzzi et al. (2019), and images were taken at a section located 50 mm from the jar wall to avoid hydrodynamic interaction. A schematic of the experimental setup is shown in Figure 1-a. For all experiments, a sampling frequency of 25 Hz was used for 40s at a resolution of 800 x 600 elemental units (pixels), with a field of view of 6 x 8 mm, and a shutter frequency of 800 µs. For these conditions, the pixel size was 10 µm and a total of 1000 images were obtained at time intervals of 40 ms (milliseconds) from t_0 to t_n, with n changing from 1 to 1000 (Figure 1-b).

For the Particle Image Velocimetry (PIV) evaluation, *Image-Pro Plus®* software was used to analyse the images, i.e. conversion from 2^8 to 2^1 bits (i.e. from 256 grayscale to black & white image), enhancement, measurement and tracking of aggregates from centroid distances d_0 to d_n, with n varying from 1 to 1000 frames, as shown in Figure 1-c.

Only aggregates with vertically projected cross sectional areas larger than 200 pixels and sizes greater than 15 pixels were chosen for accuracy in accordance with Chakraborti et al. (2003), Moruzzi and Silva (2018) and Moruzzi et al. (2019). Data were statically analysed for 95% significance.

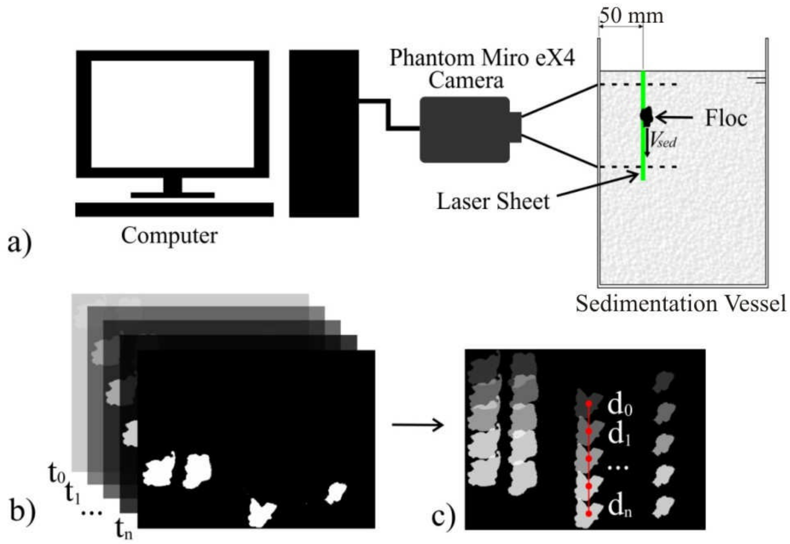

Figure 1 – (a) Schematic of the experimental arrangement used in the experiments; (b) image pack screened from time intervals from t_0 to t_n; and (c) tracking aggregates distances from d_0 to d_n using Particle Image Velocimetry (PIV) tool.

2.3 Fractal aggregate features

The three-dimensional fractal dimension (D_f) for Al-kaolin aggregates was considered individually based on Jiang and Logan (1991) and Jarvis et al. (2005):

$$N = b\left[\frac{d_f}{d_p}\right]^{D_f} \qquad (1)$$

where D_f is the three-dimensional fractal dimension for individual Al-kaolin aggregates, d_p is the primary particle size (m), here determined from the median size (d_{50}) of primary kaolin particle size distribution, d_f is the floc size (m), N is the number of particles of size d_p per floc of size d_f and b is the structure factor which comprises the packing and shape factors for aggregates and primary particles, as introduced by Bushell (2002).

The number of pixels counted in the floc area was considered representative of N from Equation 1, as it agrees with the median size (d_{50}) of around 10 µm, discussed later on this paper. The volume of the fitted ellipsoid of revolution (E) to the aggregate was used to derive the fractal dimension. This was calculated by rotating the encased ellipsoid around the longest size of E (d_{max}) limited by the smallest dimension (d_{min}), as proposed by Chakraborti et al. (2000). From these data, the three-dimensional fractal dimension (D_{fp}) was calculated for the set of aggregates, fitting the areas (A) and volumes (V) with aggregate longest length ($d_{max.}$) in *log-log* plots, using Equations 2 and 3, respectively:

$$A \sim d_{max.}{}^{D_{fp}'} \qquad (2)$$

$$V \sim d_{max.}{}^{D_{fp}} \qquad (3)$$

where A is the projected floc area on the image plane, $d_{max.}$ is the longest dimension of the floc (m), D_{fp}' is the two-dimensional fractal dimension for the set of aggregates, V is the volume of the ellipsoid containing the floc (m^3) and D_{fp} is the three-dimensional fractal dimension for the set of aggregates.

Finally, Equation 4 recently proposed by Moruzzi et al. (2020) was applied to determine the three-dimensional fractal dimension per aggregate (D_f), based on the ratio D_{fp}/D_{fp}' from the entire aggregate population and on 2D fractal dimension calculated individually:

$$D_f = \frac{D_{fp}}{D_{fp'}}\left(\frac{LogN}{Log\left(d_{max}/d_p\right)}\right) \quad (4)$$

The key assumption here is that the D_{fp}/ D_{fp}' ratio, determined from the entire aggregate population, could be applied to convert 2D to 3D fractal dimensions for individual aggregates using images. This has never been described before in the literature; however it is expected that the entire population of aggregates can provide good approximations for the shape of individual flocs.

The density of the aggregates was determined individually from the mass balance between floc, particle and voids occupied by the liquid (Jiang and Logan, 1991and Johnson et al., 1996):

$$\rho_f = \rho_l + \left(b\left(\frac{d_f}{d_p}\right)^{D_f-3}\left(\rho_p - \rho_l\right)\right) \quad (5)$$

where ρ_f is the density of aggregate (kg·m^{-3}), ρ_l is the density of water (kg·m^{-3}) and ρ_p is the density of the primary particle (kg·m^{-3}).

It is important to note that although Equation 5 describes density in terms of three-dimensional fractal dimensions, it is still assumed that primary particles are perfect spheres, as pointed by Vahedi and Gorczyca (2014). Furthermore, it was also assumed that the entire aggregate size could be represented as a homogeneous aggregation of mono-sized primary particles.

Sphericity (Ψ) and aspect ratio (i.e. the larger and shorter aggregate length ratio) were also determined, with the value of 1 representing the shape of perfect sphere for both cases (Jarvis et al., 2005). The size of each aggregate and their associated measured velocities obtained from the experiments were also used to determine the dimensionless Reynolds number (Re) for Al-kaolin aggregates:

$$Re = \frac{\rho_l d_f V_{exp}}{\mu} \quad (6)$$

where Re is the dimensionless Reynolds number, V_{exp} is the measured Al-kaolin aggregate terminal velocity by PIV ($m \cdot s^{-1}$) and μ is the absolute viscosity ($N \cdot m^{-2} \cdot s$).

Experimental velocities of fractal aggregates were compared with the modelling approach in a wide range of fractal dimensions, through the well-known Stokes' law for settling velocity modified by a dimensionless shape factor:

$$V_{calc} = \frac{\Delta\rho g {d_f}^2}{\theta 18\mu}\text{, valid for Re < 1 and } d_f < 1\text{mm, so that Cd=24/Re} \quad (7)$$

where $\Delta\rho$ is the differential density of aggregate and water, also named as aggregate buoyant density, ($kg \cdot m^{-3}$) and θ is the shape factor (dimensionless) that comprises all limitations resulting from simplifying assumptions such as: primary particles being compact and perfectly sphere-shaped with homogeneous size, aggregates being perfect shapes and impervious spheres, porosity being homogeneous in aggregates, aggregates presenting mono structures, drag coefficient (Cd) being constant and represented by 24/Re for Re < 1.

The drag coefficients for Al-kaolin fractal aggregates were also calculated, based on fractal homogeneous aggregate porosity ($\mathcal{E}$) as initially proposed by Jiang and Logan (1991), here adapted for the encased ellipsoid (E).

$$Cd = \frac{4}{3}\frac{\Delta\rho\ d_f\ g\ (1-\mathcal{E})}{\rho_f {V_{exp}}^2} \quad (8)$$

$$\mathcal{E} = 1 - b.\left(\frac{d_f}{d_p}\right)^{D_f-3} \quad (9)$$

where $\mathcal{E}$ is the Al-kaolin aggregate porosity.

3- Results and Discussion

3.1 Physical attributes

Figure 2-a shows the heterodisperse nature of dry kaolin powder with size distribution ranging from 1 to 100 μm, and median size (d_{50}) of around 10 μm, which is in agreement with the findings of other researchers (e.g. Aparício et al., 2004; Zbik and Smart, 1998). This result reinforces the hypothesis that the assumption of homogeneous and perfectly sphere-shaped primary particles is an oversimplification of a more complex shape and size distribution. Although the pixel size of 10 μm, used here, could be assumed to represent kaolin median size for volume distribution, using only one fractal dimension for flocs would result in an unrealistic high-density aggregate. Aggregates cannot be presumed as a sum of side-by-side primary particles, but a complex structure with multi-scale voids occupied by water and Al-kaolin precipitates (Vahedi and Gorczyca, 2014). As described by Gorczyca and Ganczarczyk (1999), fractal aggregates are the result of primary particles attaching onto pre-formed flocs with different levels of aggregation, leading to different sizes and pore populations within aggregates, i.e. *flocculi*, microflocs and flocs aggregates. Furthermore, Yu et al. (2015) found that when the coagulant is added to the suspension, flocs grew rapidly as primary particles enmesh within the hydroxide precipitate during the flocculation. Consequently, floc aggregates have different primary particle concentrations within fractal aggregates, and therefore, the density calculated using only one fractal dimension for flocs does not reflect the complex multilevel floc structure.

In order to overcome this issue, the cross sectional area of aggregates was analysed to determine kaolin within its structure, by performing image analysis based on different level of brightness. For this purpose, aggregates formed by Alum only were compared to those formed by Al-kaolin aggregates, making it possible to define the multi threshold level for brightness.

Figure 2-b shows an example of the aggregate structure formed by kaolin (marked in yellow) and alum gel (marked in red). Similar analysis was performed in several images and results have shown that the kaolin effective cross-sectional area is about 20 % of the total cross-sectional area average. This made it possible to calculate the floc effective bulk density (ρ_f) of 1,300 kg·m^{-3}, based on relative quantities of Alum and kaolin within flocs. This finding is in agreement with the results reported by Tambo and Watanabe (1979).

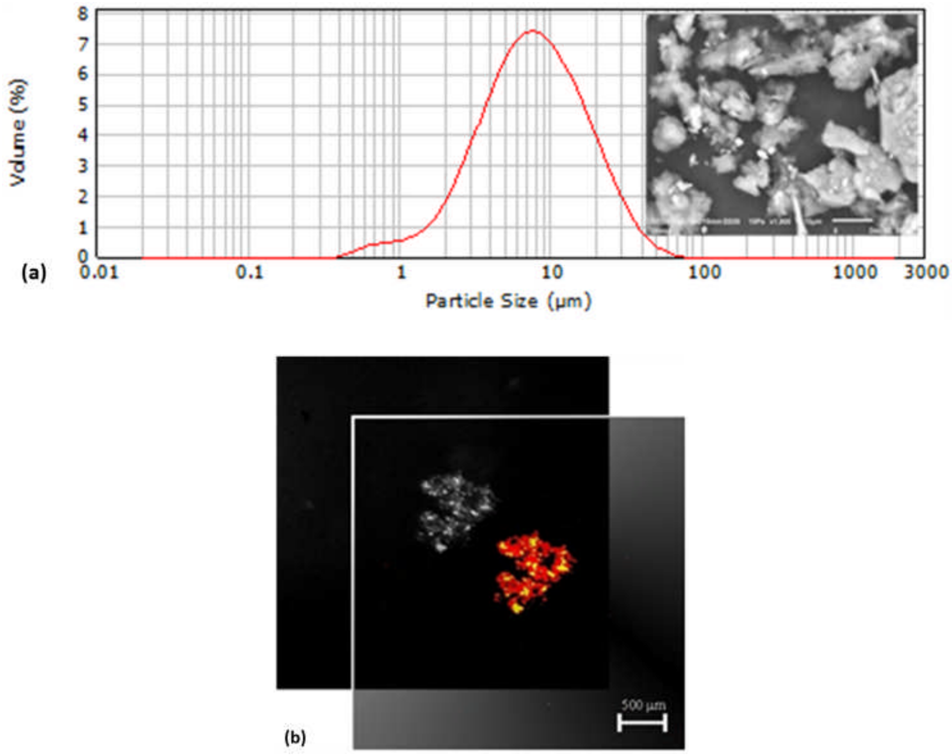

Figure 2 – (a) Volume frequency distribution for dry kaolin powder used as primary particles in the tests. The image in the right hand side of (a) refers to (SEM) taken as sample from kaolin, as dry material. (b) Example of aggregate formed by kaolin and alum. Background shows original image and front image shows kaolin highlighted in yellow within aggregate structure of Alum in red.

Figure 3-a shows an example of one of the images used to characterize the aggregate, 5 minutes after flocculation had finished, i.e. during sedimentation. It is clear that the morphology of the aggregate formed after flocculation cannot be explained by Euclidean geometry and by the assumption of impermeable spheres. Furthermore, the asymmetrical shape of aggregates can also be observed. The shape and the existence of voids inside the floc may alter the effective density of the aggregate, influencing the terminal velocity of the floc. Figure 3-b shows an example of one of the 118 tracked Al-kaolin aggregates monitored during sedimentation.

Figure 4 shows the value of two and three-dimensional fractal dimensions for the entire population of aggregates in the experimental data, according to Equations 2 and 3. The slopes of the fitted trend lines, i.e. 2.35 and 1.50, represent the three and two-dimensional fractal dimension for the set of aggregates respectively, which is compatible with the findings of Chackraborti et al. (2003) and Johnson and Logan (1996). A structure factor of 0.74 was determined from the best fit line intercept of Figure 4-b.

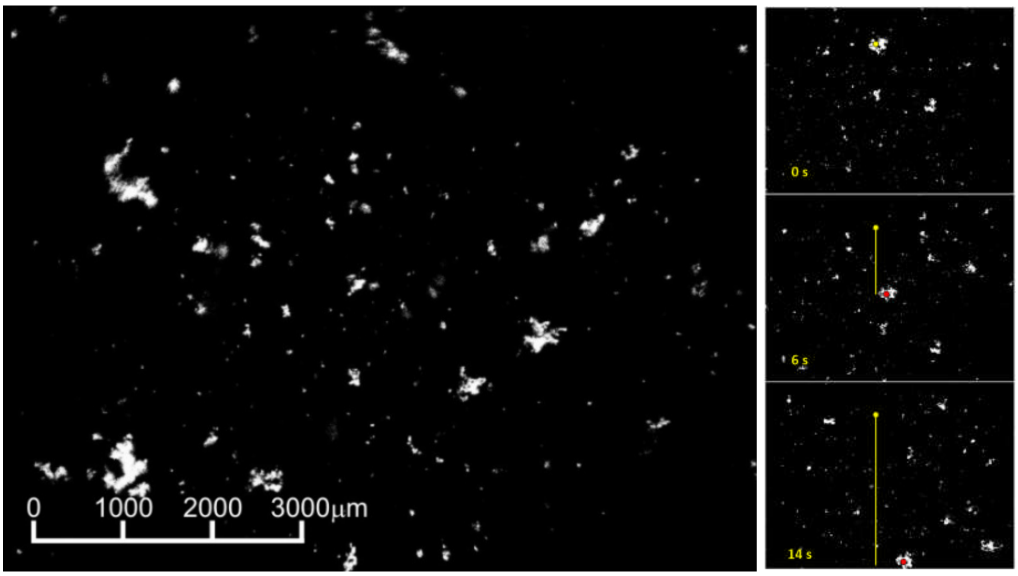

a) **b)**

Figure 3 – (a) An example of Al-kaolin fractal aggregates image obtained after the flocculation at 15 x magnification; and (b) example of fractal aggregate tracking during sedimentation for frames extracted at 0, 6 and 14 s, 4 x magnification.

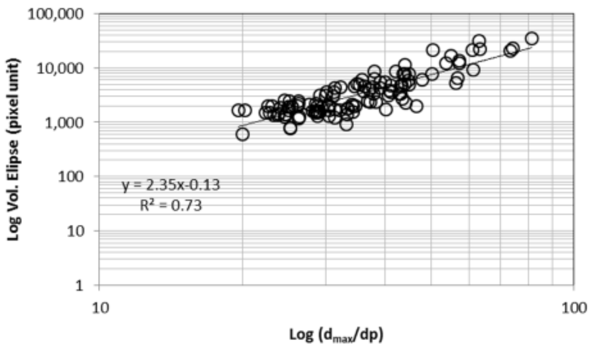

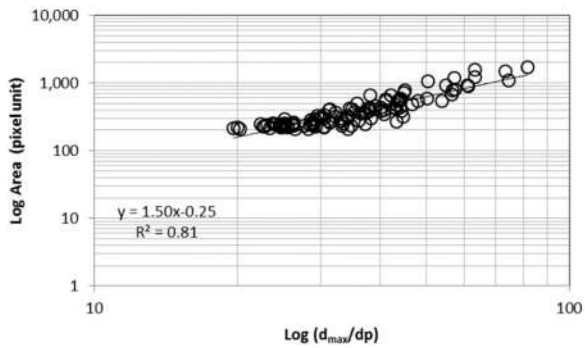

a) **b)**

Figure 4 - Fractal dimension obtained from image analysis based on the set of aggregates, (a) three-dimensional fractal dimension (D_{fp}) and (b) two-dimensional fractal dimension (D_{fp}'), calculated for the entire population of aggregates by the slope of *Log-Log* plot. Moruzzi et al. (2020).

The frequency distribution of the dimensionless aggregate sizes, i.e. the d_{max}/d_p ratio, can be observed in Figure 5. It can be seen that 86% of the measured aggregates were within the range of $30.0 \leq d_{max}/d_p \leq 50.0 \pm 2.2$, that is, their longest lengths were between 30 and 50 times larger than the mean size of primary particles of kaolin (d_{50} of 10 μm). The distribution of the fractal dimension, D_f, as determined individually for the aggregates, can be seen in Figure 6. Almost 70% of the measured D_f were within in the interval of 2.60 – 2.70 ± 0.02, which deviates from the 2.35 fractal dimension calculated from the entire population of aggregates (Figure 4-a). However, there is no consensus on what approach yields the most accurate estimates of fractal dimensions (Chakraborti et al., 2000). Later discussion in this paper will show how these two approaches relate to each other. Sphericity (Ψ) of ordinary Al-kaolin aggregates was determined individually, and found to be around 0.58 ± 0.02 for all 118 measured average aggregates, based on the encased ellipsoid (E), with average aspect ratios of about 2.7. Such results indicate irregular geometries, which cannot be adequately explained by regular plane geometry, and these findings agree with those presented by Vahedi and Gorczyca (2012).

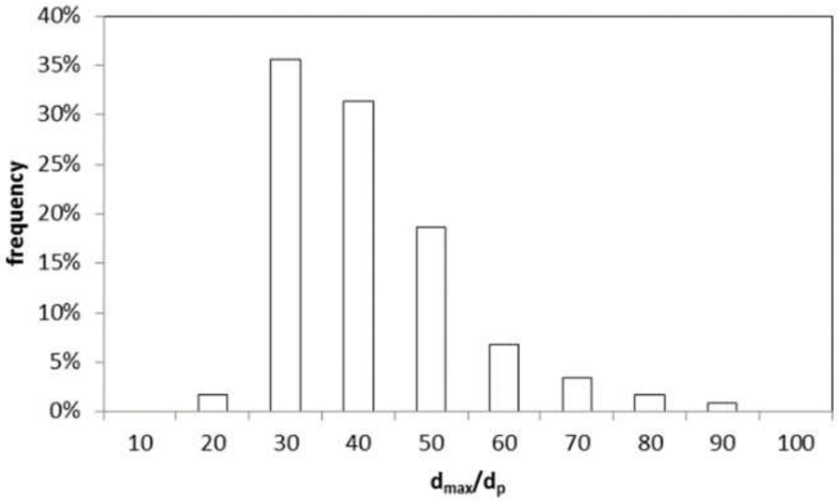

Figure 5 - Discrete distribution of dimensionless aggregate sizes, expressed by the ratio d_{max}/d_p.

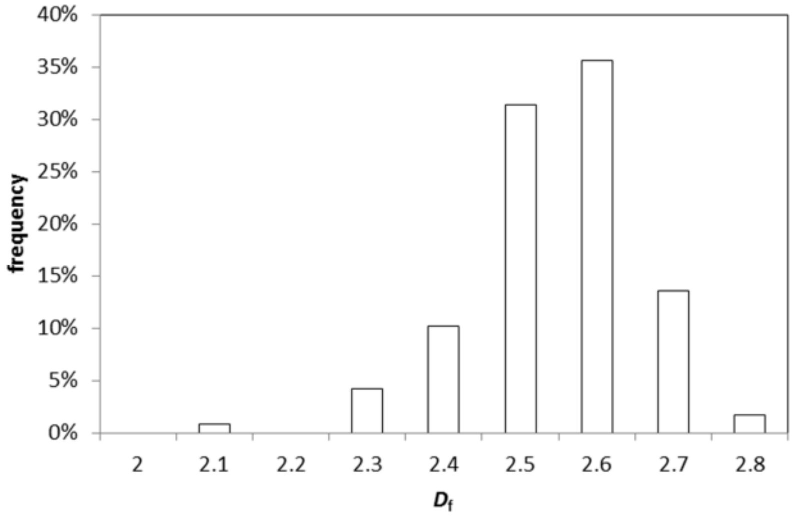

Figure 6 - Discrete distribution of the fractal dimension (D_f) determined by individual aggregates.

In Figure 7, the three-dimensional fractal dimension is plotted against the longest length of fractal aggregate size. It is clear that shape is independent of aggregate size for the entire population of large aggregates (triangles in Figure 7), i.e. there is no dominant fractal dimension for large Al-kaolin aggregates. This is in agreement with the findings of Jiang and Logan (1991) who identified an overlap in fractal dimension for aggregates formed from Brownian motion and differential sedimentation, despite the different aggregates sizes in which those mechanisms are likely to be dominant. The results from Figure 7 are in agreement with the findings presented by Vahedi and Gorczyca (2012) who considered a non-linear behaviour for D_f and floc size, and reinforced that the variety of aggregation mechanisms, kinetics (aggregation and breakage) and the sort of primary particles are some of the possible reasons why flocs with the same size may exhibit many different structures and different fractal dimensions. However, a closer look at particular and smaller range of aggregates, ranging from 180 to 300 μm (black circles in Figure 7), allows the identification of a linear relationship between D_f and size, which is in accordance with the data presented by Vahedi and Gorczyca (2014). Furthermore, Vahedi and Gorczyca (2012) have also shown greater dispersion of D_f for large flocs, with D_f varying from 2.3 to 2.9 for floc size of 200 μm, for example.

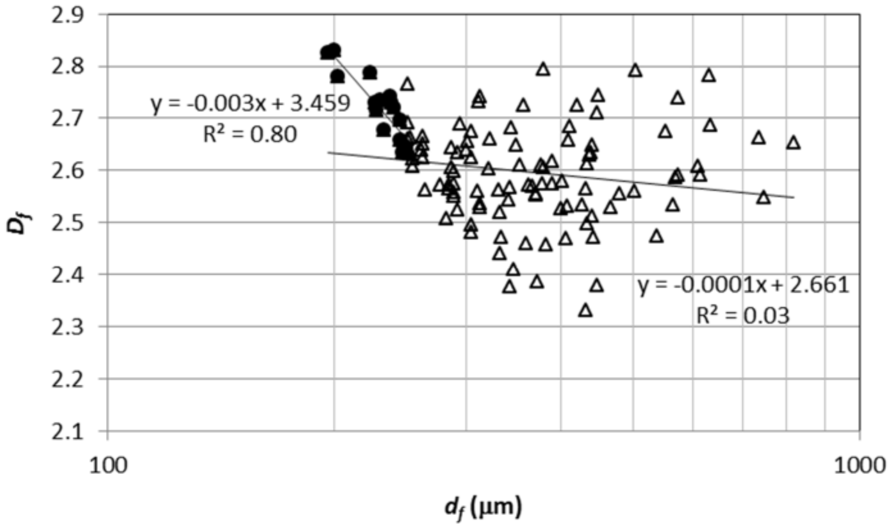

Figure 7 – Variation of the three-dimensional fractal dimension calculated individually with the longest length of fractal aggregate size. Triangles (Δ) refer to the entire population of large aggregates and black circles (•) refer to subset of longest length between 180 and 300 μm.

Figure 8-a shows the values of density (ρ) determined from the fractal dimensions per aggregate (D_f), using Equation 5. Individual aggregate densities vary from 1,020 to 1,140 kg·m$^{-3,}$ for D_f within the range of $2.3 \leq D_f \leq 2.7$ and size range in the interval $20 \leq d_f/d_p \leq 80$. The density of the aggregates, with an average of 1,068 ± 4 kg·m^{-3}, seems to slightly vary with the d_f/d_p ratio and also depends, to a lesser extent, on the fractal dimension (D_f). The aggregate densities scatter in a wide range of D_f and they seem to be slightly dependent on size for large aggregates. Hence, several densities can be found for the same size, as also

shown when the D_f values are calculated individually, which is in agreement with the results presented by Vahedi and Gorczyca (2012). The reason for this probably lies in the fact that the shape and compactness of the flocs also have an influence on density. Thus, for Al-kaolin aggregates in the range of 180.0 to 816.0 ± 2.2 μm, there are a variety of shapes and densities, which are independent in their size only, when aggregates are considered individually. However, a linear behaviour can be observed, in the range of 180 to 300 μm, which is in accordance with previous analysis and suggests that a large variation is expected for bigger aggregates.

Another analysis for the density and size relationship can be performed by rearranging Equation 5, so that results can be expressed in the form of Equation 10, presented by Gregory (1997) for the entire population of flocs. In this case, Equation 5 transforms to Equation 11, written in *Log-Log* format.

$$\rho_f = B{d_f}^{-y}, \quad \text{for } y = 3 - D_f \qquad (10)$$

$$Log\left(\frac{\rho_f - \rho_l}{\rho_p - \rho_l}\right) = Logb - yLog\left(\frac{d_f}{d_p}\right) \qquad (11)$$

Figure 8-b was plotted using Equation 11 applied to the same data used in Figure 8-a. It is clear that the entire population of aggregates behave as expected by Gregory (1997), and from the best fit line (in green) it is possible to determine that *y* of Equation 11 equals to 0.65. This results in D_f of 2.35, which is indeed the three-dimensional fractal dimension for the entire population of flocs, and agrees with the fractal dimension previously calculated using Equation 2 and shown in Figure 4-a. Therefore, 3D fractal dimension for the whole population of aggregates can be derived from the density and size relationship determined from fractal dimension calculated individually.

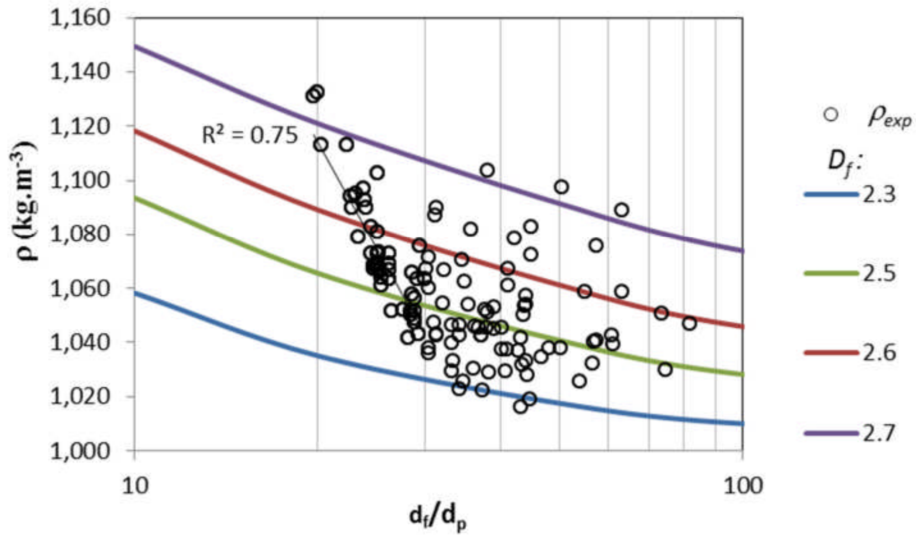

(a)

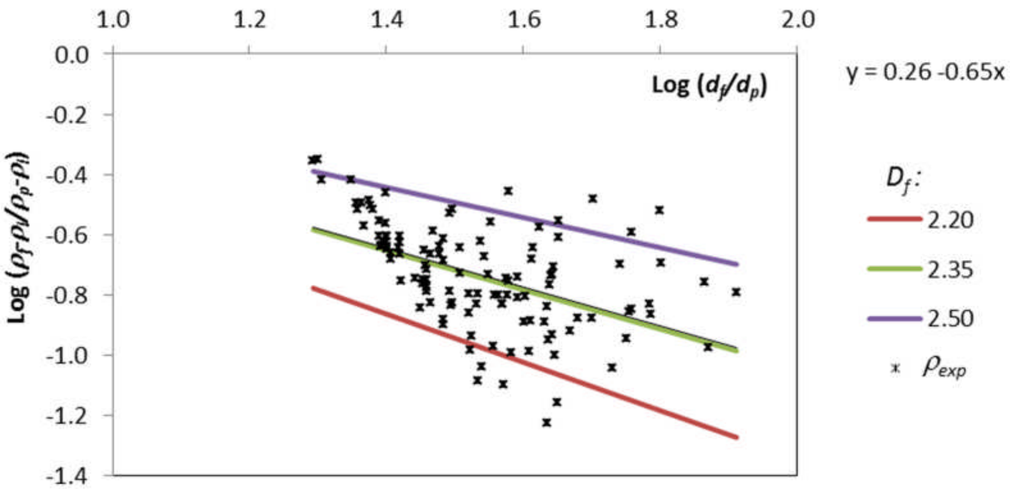

(b)

Figure 8 – (a) Changes of calculated density (ρ), determined from fractal dimension of individual aggregates, with the d_f/d_p ratio, using Equation 5. The coloured curves represent the calculated density for three-dimensional fractal dimensions (D_f) of 2.3, 2.5, 2.6 and 2.7. (b) *Log-log* plot of density measurements against the d_f/d_p ratio using Equation 11.

3.2 Settling velocity

Figure 9-a, presents the discrete distribution of aggregate velocities during sedimentation. In general, the measured velocities of the selected 118 slow-settling Al-kaolin aggregates ranged from 1.0×10^{-4} to $2.0\times10^{-3} \pm 3\times10^{-5}$ $m\cdot s^{-1}$. It was verified that 75% of the aggregates had settling velocities in the range of 3.0×10^{-4} to $5.0\times10^{-4} \pm 3\times10^{-5}$ $m\cdot s^{-1}$ and 10% of the aggregates settled at a velocity greater than 1.0×10^{-3} $m\cdot s^{-1}$, which is equivalent to the settling rate expected for a sphere of 170 μm size and ρ_f of 1,300 $kg\cdot m^{-3}$, far lower than the average floc size of 360 μm. However, 15% of the aggregates settled with velocity of less than 2.0×10^{-4} $m\cdot s^{-1}$. On average, the settling velocity for Al-kaolin aggregates was found to be 3.5×10^{-4} $m\cdot s^{-1}$ (i.e. 30 $m\cdot day^{-1}$), which is slower than common values adopted for hydraulic loading rate of conventional settling tanks (around 4.6×10^{-4} $m\cdot s^{-1}$, i.e. 40 $m\cdot day^{-1}$), explaining why those large aggregates can be dragged out of sedimentation tanks. Also, settling velocities here measured for Al-kaolin aggregates were considerably lower than those measured by Vahedi and Gorczyca (2012), probably due to the denser primary material (lime) used to form flocs, and much lower than those measured by Johnson et al. (1996), who have studied smaller flocs sizes.

Floc-floc collision was not observed during these experiments, perhaps because it is less likely to occur in low-concentration suspension, as also observed by Goula et al. (2008). However, it must be highlighted that higher suspended particles can favour aggregate collisions, potentially increasing floc size and changing settling velocities during sedimentation (Zhao et al., 2018; Shi et al., 2019).

The intrinsically slow-settling Al-kaolin aggregates investigated here certainly influences the average values presented and contributes to the observed difference, once the focus was on slow settling of large aggregates. Furthermore, aggregates have far from the ideal impermeable spheres assumed for the Stokes' law simplification and this can also explain such behaviour, as previously mentioned.

It is clear from Figure 9-b that Re values calculated from experimental measurements are lower than those back-calculated from Stokes' law for spheres using a drag coefficient (Cd) equal to 24/Re. The overestimation for Re of large latex spheres (< 160 μm) was also observed by Chakraborti and Kaur (2014), who concluded that greater deviation may be expected as particle size increases, probably due to an increase in drag coefficient with relatively large-particle Re numbers compared to the value used in Stokes' law. Here, those effects on drag coefficient are likely more significant, as fractal aggregates were calculated individually. Furthermore, fractal aggregates formed from kaolin primary particles arise from more complex mechanisms, such as hydrodynamic effects, than those formed from latex spheres, and so, the observed deviation for Re is even higher than those reported by Chakraborti and Kaur (2014).

Figure 9-b also shows that most Re values were less than 0.2, thus making the Stokes' law modified by a shape factor applicable as presented by Wang (1988) and also used by Vahedi and Gorczyca (2012).

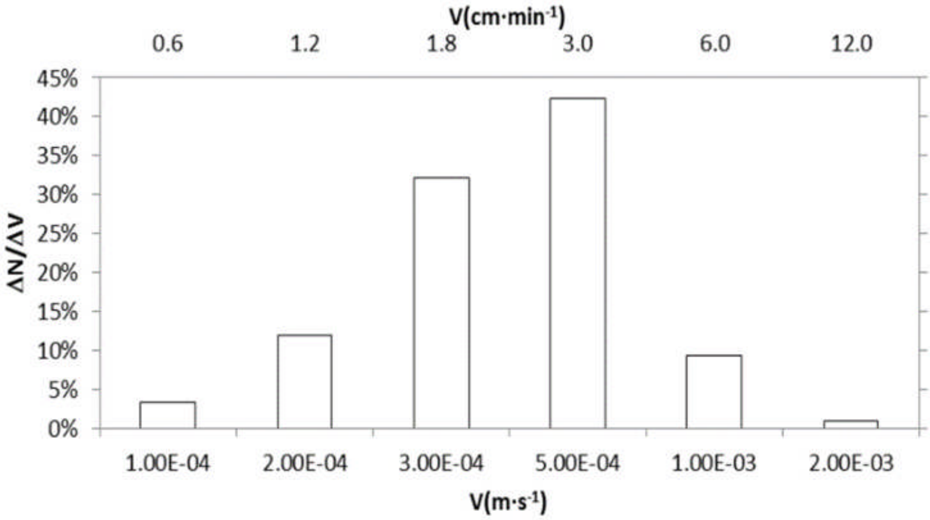

(a)

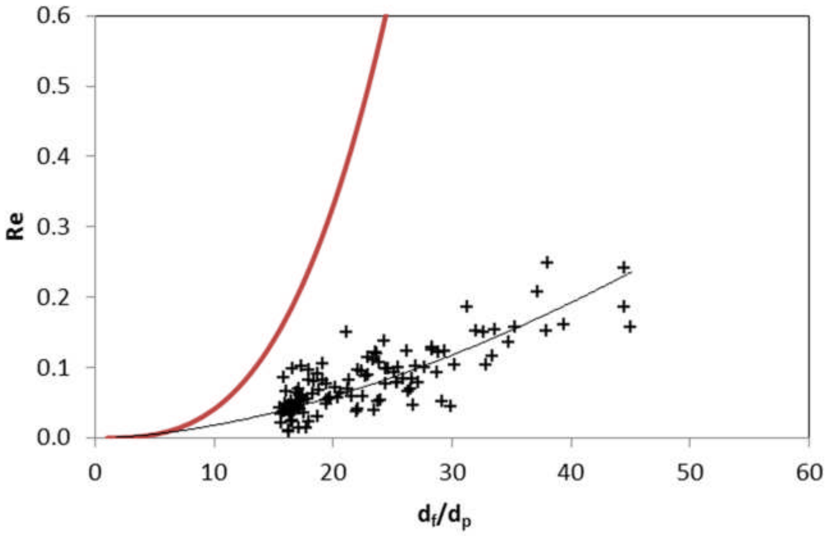

(b)

Figure 9 – (a) Discrete distribution for settling velocities of Al-kaolin aggregates with measured average size ranging from 150 to 450 ± 1.3 μm and (b) calculated dimensionless Reynolds number (Re) from experiments and back-calculated Re values from Stokes' Law (continuous red line) against dimensionless aggregate size (d_f/d_p).

Figure 10 shows the experimental results, based on settling velocities (*V*) and normalised sizes (d_f/d_p). Coloured continuous lines describe the relation $V \approx (d_f/dp)^2$, limited by the range of $5 \leq \Delta\rho/\theta \leq 35$ kg·m^{-3}, as Equation 7. The best fit lines in black refer to the minimum least square relation between aggregate velocity and size for two subsets of data: i) the entire set of data, drawn in continuous black line, where the slope is 0.73 ($V \approx (d_f/d_p)^{0.73}$); ii) the subset limited by the average size $100 \leq d \leq 200$ μm, dashed line, where the slope is 1.30 ($V \approx (d_f/dp)^{1.30}$).

As observed above for fractal dimension and density, Al-kaolin aggregates with similar sizes can have different settling velocities. This is also in agreement with results reported by Vahedi and Gorzzyka (2012), who observed several settling velocities for one aggregate size. It is clear that experimental velocities of Al-kaolin aggregates, for average size (*d*) within 150 to 450 ± 1.3 μm, are predominantly (95%) encased within the limits of the lines $5 \leq \Delta\rho/\theta \leq 35$ kg·m^{-3} (with slope of 2) using Equation 7, i.e. in the shape factor interval of $2 \leq \theta \leq 14$. A θ value equal to one would be expected for perfectly spherical-shape and impermeable aggregates, settling in accordance with Stokes' law for Re < 1, i.e. at drag coefficient of 24/Re. This means that assumptions based on Stokes' law do not represent large Al-kaolin aggregates and settling velocities were over-predicted from 2 to 14 fold. Using the raw data published by Tambo and Watanabe (1979) for primary particles of clay-aluminium of 3.5 μm size, Bushell et al. (2002) found a drag and structure factor coefficient of 5.42, which derives from actual velocities lower than the Stokes' law prediction. Therefore, aggregates took on non-spherical shapes resulting in increased drag force and, consequently, had slow settling rates compared to spherical particles, as pointed out by Bushell et al. (2002).

According to the Stokes' law, the terminal velocity of settling aggregates is proportional to size squared, as given by Equation 7. Results of the analysis here have shown that density and fractal dimension can be related in a wide range of size, and therefore, multiple settling velocities were observed for a given floc size. For the entire population of the aggregates, the experimental velocity was found to vary with size to the power of 0.73 (black line in Figure 10), which agrees with results presented by Tambo and Watanabe (1979), who found values between 0.5 and 1.0. However, for the average size range of 100 – 200 μm, the exponent for size is found to be 1.30 (dashed black line in Figure 10), in accordance to the exponent given by $D_f - 1$, presented by Vahedi and Gorczyca (2012).

Therefore, it is important to note that the shape factor, used here to encase experimental values in the border limit of Stokes law's theoretical settling velocities, comprises a wide range of simplifications over porosity, permeability, size and shape. In general, results have shown that large fractal aggregates settled too slowly for Stokes' law to apply, and they may behave differently for the same size.

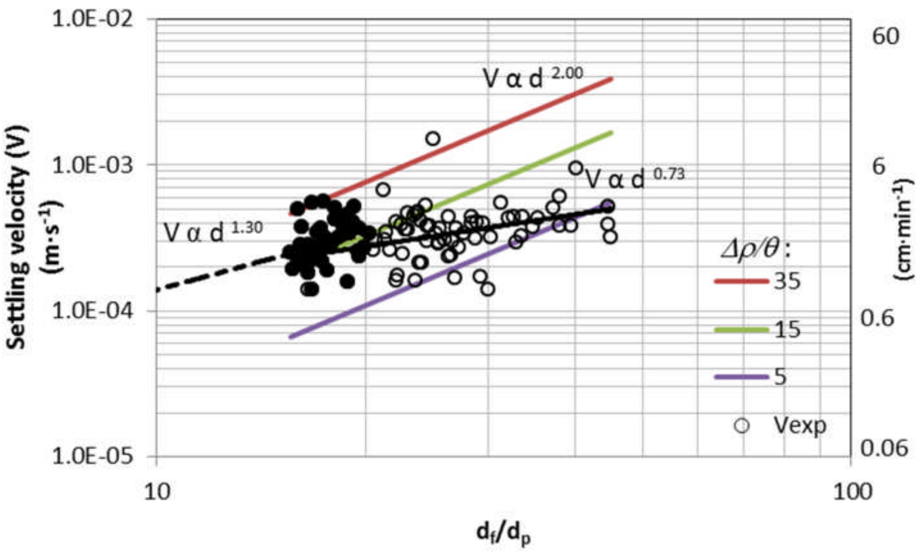

Figure 10 - Settling velocities for Al-kaolin fractal aggregates against dimensionless size (d_f/d_p). Coloured lines represent the limits of $\Delta\rho/\theta$ with $V \approx (d_f/d_p)^2$ from Equation 7. The continuous black line represents the best fit for all measured data, and the dashed line is the best fit for a subset of aggregate sizes.

Figure 11 shows the relationship between Reynolds number (Re) and drag coefficient (Cd), determined from experimental results as described by Equations 6 and 8, respectively. The inversely proportional relation between Cd and Re was confirmed, and a proportionality constant of 56 was determined from the fitted line. Tambo and Watanabe (1979) calculated the proportionality constant of 45 for Ψ of 0.80, confirming that deviation from sphericity leads to a higher drag coefficient, despite the fact that both shape and orientation of aggregates in flow affect results, as pointed by Bushell et al. (2002).

Results in Figure 11 also confirmed that for Al-kaolin aggregates, the impact of aggregation of non-sphere primary particles of 10 μm median on the hydrodynamics resulted in the increase of drag forces, when compared with perfect spheres of the same density settling according to Stokes' law. The results, discussed in previous paragraphs, indicated that Al-kaolin aggregates are asymmetrical, as the three-dimension fractal dimensions presented in Figure 7 were found to be independent of size, or sphericity (Ψ) and far from spherical shape (Ψ = 0.58) with aspect ratio of about 2.7. Therefore, these aggregates may spin or wobble as they settle, as also mentioned by Bushell et al. (2002). Finally, the results have also confirmed that permeability did not play an important role on high fractal dimension aggregates, as also revealed by Gregory (1997) and Bushell (2002), especially as voids are potentially filled with hydrolysed coagulant species (Vahedi and Gorczyca, 2014).

In general, the results presented here suggest that the settling velocity of Al-kaolin large fractal aggregates is influenced by shape, density, and porosity as well as size, and that these features may change the equilibrium configuration between the gravitation and drag forces acting on the particle during its sedimentation. Finally, it must be stressed that the high ionic strength water here studied (0.1 M $NaHCO_3$) means that electrical effects would be negligible and the diffusion of the large flocs would be insignificant. Therefore, sedimentation velocity is not remarkably affected by particle charge (Gregory, 1997), and for this reason, particle charge was not investigated in this study.

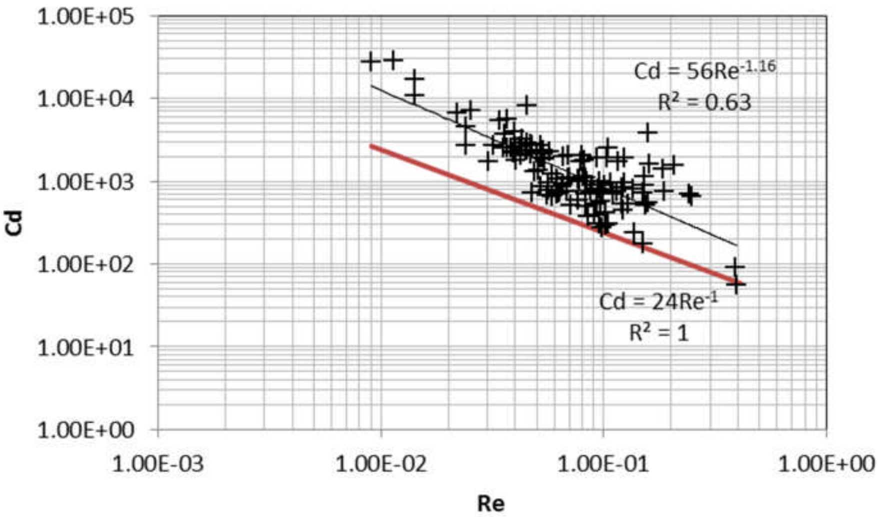

Figure 11 – Drag coefficient determined from experimental results. The black line is the best fit to experimental data whilst the red line was determined using drag coefficient (Cd) of 24/Re for Re < 1.

Conclusions

In this paper, large slow-settling Al-kaolin fractal aggregates' features and Re numbers were determined using a non-intrusive image technique, and were found to differ from values reported in other studies on obtaining aggregate characteristics from sedimentation. This approach avoids the assumption of an explicit relationship between drag coefficient and aggregate size.

It was proposed that the 3D fractal dimension for the whole population of aggregates can be derived from the density and size relationship, using fractal dimensions calculated individually, by means of the rearrangement of the mass balance equation.

It was found that Al-kaolin large aggregates may exhibit different settling velocities for the same size and the velocities based on Stokes' law do not accurately represent large aggregates, where settling velocities were over-predicted from 2 to 14 fold.

The impact of aggregation of non-spherical kaolin primary particles of 10 μm median on Al-kaolin aggregate hydrodynamics results in an increase of the drag force, when compared with perfect spheres of same density, settling in accordance with Stokes' law. The inversely proportional relation between Cd and Re was confirmed, and a proportionality constant of 56 ($Cd = 56/Re$) was determined graphically, compared to the Stokes' relation of $24/Re$.

Therefore, it was found that Al-kaolin large, heterodisperse and multi-shape aggregates can settle sufficiently slowly for Stokes-type expressions to apply. The asymmetrical shape and the size-density relatively independence here verified for large aggregates play an important role on Al-kaolin large aggregates with slower settling velocities. Evidently, more research is needed in order to better understand the complex mechanisms behind the settling rates of large fractal aggregates with slow settling velocities. For example, those mechanisms referring to the effects of collision and restructuring during sedimentation and flocs alignment with flow direction should be investigated.

Acknowledgements

Rodrigo B. Moruzzi is grateful to São Paulo Research Foundation (Fundação de Amparo à Pesquisa do Estado de São Paulo—FAPESP) Grant 2017/19195-7, to CNPq for fellowship Grant 301210/2018-7 for financial support and to University College London for the academic visitor contract.

References

Aparício, P., Pérez-Bernal, J. L., Galán, E., Bello, A., 2004. kaolin fractal dimension. Comparison with other properties. Clay Minerals. v. 39, p. 75-84.

Bushell, G. C., Yan, Y. D., Woodfield, D., Raper, J. U. D. Y., Amal, R. O. S. E., 2002. On techniques for the measurement of the mass fractal dimension of aggregates. Advances in Colloid and Interface Science, 95(1), 1-50.

CETESB, 2015. Qualidade das águas superficiais no estado de São Paulo 2014. Available at: https://cetesb.sp.gov.br/aguas-interiores/wp-content/uploads/sites/12/2013/11/Cetesb_QualidadeAguasSuperficiais2014_ParteI_vers%C3%A3o2015_Web.pdf

Chakraborti R.K., Kaur J., 2014. Noninvasive Measurement of Particle-Settling Velocity and Comparison with Stokes' Law. Journal of Environmental Engineering. 5;140(2):04013008.

Chakraborti, R.K., Atkinson, J.F., Van Benschoten, J.E., 2000. Characterization of alum floc by image analysis, Environmental Science and Technology 34, 3969–3976.

Chakraborti, R.K., Gardner, K.H., Atkinson, J.F., Van Benschoten., J.E., 2003. Changes in fractal dimension during aggregation. Water Res, 37, 873–883.

Eman N, A., Suleyman A, M., Hamzah M, S., Md Zahangir, A., & Mohd Ramlan M, S., 2010. Production of natural coagulant from Moringa oleifera seed for application in treatment of low turbidity water. Journal of Water Resource and Protection, 2010.

Goula, A. M., Kostoglou, M., Karapantsios, T. D., & Zouboulis, A. I., 2008. A CFD methodology for the design of sedimentation tanks in potable water treatment: Case study: The influence of a feed flow control baffle. Chemical Engineering Journal, 140(1-3), 110-121.

Gregory, J., 1997. The density of particle aggregates. Water Science and Technology, v. 36, n. 4, p. 1-13.

Jarvis, P., Jefferson, B., Gregory, J., Parsons, S.A., 2005. A review of floc strength and breakage. Water Res., 39, 3121–3137.

Jiang Q, Logan B.E., 1991. Fractal dimensions of aggregates determined from steady-state size distributions. Environmental Science & Technology, 25(12):2031-8.

Johnson, C.P., Li, X., Logan, B.E., 1996. Settling velocities of fractal aggregates. Environ. Sci. Technol., 30, 1911-1918.

Johnson, M., Peakall, J., Fairweather, M., Biggs, S., Harbottle, D., & Hunter, T. N., 2016. Characterization of multiple hindered settling regimes in aggregated mineral suspensions. Industrial & Engineering Chemistry Research, 55(37), 9983-9993. ISSN 0888-5885.

Li, T., Zhu, Z., Wang, D., Yao, C., Tang, H., 2006. Characterization of f loc size, strength and structure under various coagulation mechanisms. Power Technology, 168, 104-110.

Li, X. Y., Zhai, X. D., Chu, H. P., & Zhang, J. J., 2008. Characterization of the flocculation process from the evolution of particle size distributions. Journal of Environmental Engineering, 134(5), 369-375.

Liu, Z., Wei, H., Li, A., & Yang, H., 2019. Enhanced coagulation of low-turbidity micro-polluted surface water: properties and optimization. Journal of environmental management, 233, 739-747.

Moruzzi, R. B., da Silva, P. G., Sharifi, S., Campos, L. C., & Gregory, J., 2019. Strength assessment of Al-Humic and Al-kaolin aggregates by intrusive and non-intrusive methods. Separation and Purification Technology, 217, 265-273.

Moruzzi, R. B., de Oliveira, A. L., da Conceição, F. T., Gregory, J., & Campos, L. C., 2017. Fractal dimension of large aggregates under different flocculation conditions. Science of the Total Environment, 609, 807-814.

Moruzzi, R.B., Bridgeman, J. and Silva, P.A.G., 2020. A combined experimental and numerical approach to the assessment of floc settling velocity using fractal geometry. Water Science and Technology.

Moruzzi, R.B., Silva, P. A. G., 2018 Reversibility of Al-kaolin and Al-Humic aggregates monitored by stable diameter and size distribution. Brazilian Journal of Chemical Engineering, v. 35, n. 3, p. 1029-1038.

Oliveira, A.L.de, Moreno, P., Silva, P.A.G. da, Julio, M.D., Moruzzi, R.B., 2015. Effects of the fractal structure and size distribution of flocs on the removal of particulate matter. Desalination and Water Treatment. DOI:10.1080/19443994.2015.1081833. Taylor & Francis, 1-12.

Raşa, M., & Philipse, A. P., 2004. Evidence for a macroscopic electric field in the sedimentation profiles of charged colloids. Nature, 429(6994), 857-860.

Shi, Z., Zhang, G., Zhang, Y., He, T., & Pei, G. (2019). Modeling of Flocculation and Sedimentation Using Population Balance Equation. Journal of Chemistry, 2019.

Swenson, H. A., 1965. A primer on water quality. US Department of the Interior, Geological Survey.

Tambo, N., Watanabe, Y., 1979. Physical characteristics of flocs—I. The floc density function and aluminium floc. Water Research, v. 13, n. 5, p. 409-419.

Tang, P., Greenwood, J., & Raper, J. A. 2002. A model to describe the settling behavior of fractal aggregates. Journal of colloid and interface science, 247(1), 210-219.

Vahedi, A., Gorczyca, B., 2012. Predicting the settling velocity of flocs formed in water treatment using multiple fractal dimensions, Water Res. 46, 4188 – 4194.

Vahedi, A., Gorczyca, B., 2014. Settling velocities of multifractal flocs formed in chemical coagulation process. Water Research, v. 53, p. 322-328.

Wang, R. F. T., Brooks, N. H., Koh, R. C., 1988. Laboratory analysis of settling velocities of wastewater particles in seawater using holography. Environmental Quality.

Wei, J. C., Gao, B. Y., Yue, Q. Y., & Wang, Y., 2010. Strength and regrowth properties of polyferric-polymer dual-coagulant flocs in surface water treatment. Journal of Hazardous Materials, 175(1-3), 949-954.

Yu, W., Gregory, J., Campos, L. C., & Graham, N., 2015. Dependence of floc properties on coagulant type, dosing mode and nature of particles. Water Research, 68, 119-126.

Yukselen, M.A., Gregory, J., 2004. The reversibility of floc breakage, Int. J. Mineral Process. 73, 251–259.

Zbik, M.; Smart, St.C. R., 1998. Nanomorphology of kaolinites: comparative SEM and AFM studies. Clays and Clay Minerals. v. 46. n.2, p. 153-160.

Zhao, J., Wang, A., Wei, L., Ge, W., Chi, Y., & Lai, Y. (2018). Effect of kaolin on floc properties for reactive orange removal in continuous coagulation process. Water Science and Technology, 78(3), 571-577.